HHS Public Access

Author manuscript

Sci Signal. Author manuscript; available in PMC 2021 August 01.

Published in final edited form as:

Sci Signal. ; 11(554): . doi:10.1126/scisignal.aat5018.

Regulation of Cl^-_{in} signaling and ion transport by IRBIT-mediated recruitment of multiple kinases and phosphatases

Laura Vachel[1,6], **Nikolay Shcheynikov**[1,6], **Osamu Yamazaki**[1,2,6], **Moran Fremder**[3], **Ehud Ohana**[3], **Aran Son**[1], **Dong Min Shin**[4], **Ai Yamazaki-Nakazawa**[1], **Chin-Rang Yang**[5], **Mark A. Knepper**[5], **Shmuel Muallem**[1]

[1]The Epithelial Signaling and Transport Section, National Institute of Dental and Craniofacial Research, National Institutes of Health, Bethesda, MD 20892

[2]Apheresis and Dialysis Center/General Medicine, Keio University, 35 Shinanomachi, Shinjuku-ku, Tokyo, Japan. 160-0016

[3]Department of Clinical Biochemistry and Pharmacology, Faculty of Health Sciences, Ben Gurion University of the Negev, 84105 Beer Sheva, Israel

[4]Department of Oral Biology, BK 21 PLUS Project, Yonsei University College of Dentistry, Seoul 120-752, Korea

[5]Epithelial Systems Biology Laboratory, Systems Biology Center, National Heart, Lung, and Blood Institute, National Institutes of Health, Bethesda, MD 20892.

[6]Equal contributors and should be considered first co-authors.

Abstract

IRBIT is a multifunctional protein that controls the activity of IP_3 receptors and the Cl^- and HCO_3^- transporters NBCe1-B, CFTR and Slc26a6, by an unknown mechanism. IRBIT interacts with the NBCe1-B N terminus autoinhibitory domain (AID), exposing two cryptic Cl^- sensing GXXXP sites to confer regulation of NBCe1-B by Cl^-_{in}. Here, LC-MS/MS phosphoprotein analysis revealed that IRBIT controls five NBCe1-B phosphorylation sites that determine both NBCe1-B active conformations and regulation by Cl^-_{in}. Specifically, IRBIT-dependent combinatorial dephosphorylation of pS^{232}, pS^{233} or pS^{235} generated the conformations pS^{233}/pS^{235}, pS^{232}/pS^{235} or pS^{232}/pS^{233}. The pS^{233}/pS^{235} conformer was fully active, and was no longer activated by IRBIT or inhibited by Cl^-_{in}. The pS^{232}/pS^{235} conformer properties were similar to those of wild-type NBCe1-B, while the pS^{232}/pS^{233} conformer was partially active, had higher affinity for IRBIT, but retained inhibition by Cl^-_{in}. In addition, IRBIT recruited the phosphatase PP1 and the kinase SPAK to control S^{65} phosphorylation, which reciprocally affected Cl^-_{in} sensing by the ^{32}GXXXP^{36} motif. IRBIT recruited the phosphatase calcineurin and the kinase CaMKII to control phosphorylation of S^{12}, which reciprocally affected Cl^-_{in} sensing by the

Correspondence to: Shmuel Muallem.

Authors contributions: LV, NS, OY, AS, AY-N, EO performed experiments and interpreted results, MF and EO performed structural prediction, C-RY and MAK performed LC-MS/MS-based phosphoproteomics and interpreted results, DMS interpreted results, SM conceived the study, interpreted results and drafted the manuscript with contribution by all authors.

Competing Interests: All authors declare no competing interests.

Data and Materials Availability: All plasmids generated in the PIs lab and used in this study are available upon request.

^{194}GXXXP^{198} motif. S^{232}/S^{233}/S^{235} are conserved in several NBC transporters. Mutating the serines to alanines resulted in fully active transporters, while mutating the serines to the phosphormimetic aspartates resulted in inhibited transporters, suggesting that S^{232}/S^{233}/S^{235} determine whether NBC transporters are in active or inactive conformations. These findings reveal how multiple kinase/phosphatase pathways use multiple phosphorylation sites to fine tune a transport function, which have important implications for epithelial fluid and HCO_3^- secretion.

Introduction

Cl^- is the principal extracellular and intracellular anion in all vertebrate cells. Extracellular Cl^- (Cl^-_{out}) maintains bodily fluid and volume homeostasis and blood pressure and is thus fairly constant, except in disease states mainly associated with metabolic acidosis and alkalosis (1). Conversely, intracellular Cl^- (Cl^-_{in}) varies considerably between cells and changes markedly in response to cell stimulation. The resting Cl^-_{in} concentration in epithelial cells is as high as 60 mM (2–4), while in neurons and muscles it is between 5–20 mM (5, 6). When Cl^--absorbing and HCO_3^- secreting ducts are stimulated, ductal Cl^-_{in} is reduced from ~40 mM to 4 mM by basolateral membrane Cl^- extrusion at the later phase of Cl^- absorption to allow the high HCO_3^- concentration (up to 140 mM) in the secreted fluids. This is accomplished by enhancement of basolateral NBCe1-B-dependent HCO_3^- influx and luminal CFTR and Slc26a6-mediated HCO_3^- efflux and Cl^- influx (4, 7).

Cl^-_{in} is regulated by ion channels and transporters coupled to other ions, mainly Na^+, K^+ and HCO_3^-. These include the ClC (8) and ANO (9) Cl^- channels, the NaCl cotransporter NCC, the KCl cotransporters KCCs, the Na^+-K^+−2Cl^- cotransporter NKCC1 (10), the SLC26 Cl^-/HCO_3^- exchangers and channels (11, 12), and members of the SLC4 exchanger and cotransporter family (13). In turn, Cl^-_{in} regulates the cellular activity of several ions (7), intracellular pH (13), and cell volume (11), to affect membrane potential (14) and transepithelial fluid and electrolyte secretion (7). In addition, Cl^-_{in} modulates the activity of the cell volume/osmolarity-sensitive kinases, like WNK1 (15), WNK4 (16), WNK3 (17), SPAK (18), JNK and p38 (19). Cl^-_{in} regulates the activity of several transporters and channels. In addition to affecting Cl^--coupled transporters through changes in driving force, reduction in Cl^-_{in} activates NKCC1 (20), NKCC2 (21), and NCC (22) by phosphorylating the transporters, and modulates the function of various Na^+-HCO_3^- cotransporters (23) by an unknown mechanism.

Cl^--sensitive kinases can phosphorylate target proteins to increase their activity (24) or change ion channel selectivity (25). Cl^-_{in} can also directly interact with transporters to modulate their activity. Yet the mechanisms by which Cl^-_{in} is sensed to modulate the activity of ion transporters is not well understood. Analysis of CLC Cl^- channels and transporters has identified GXXXP motifs as Cl^- sensing sites, and participate in Cl^- regulation of SLC26A2 (26), NBCe1-B, and NBCe2-C (23, 27–29). In NBCe1-B, Cl^-_{in} is sensed by with two GXXXP motifs and both are required to confer inhibition of the NBCs by Cl^-_{in} between 5–60 mM. The first motif is ^{32}GXXXP^{36} located in NBCe1-B autoinhibitory domain (AID residues 1–40) and the second motif is ^{194}GXXXP^{198} (Fig. S4).

NBCe1-B and other epithelial transporters that function together with NBCe1-B to mediate epithelial fluid and electrolyte secretion, including CFTR, Slc26a6, KCC, NCC and NKCC1, are regulated by multiple kinases and phosphatases (24, 30–32). In secretory gland ducts NBCe1-B, CFTR and Slc26a6 are activated by the IRBIT protein (IP_3 receptor binding protein released with IP_3) (23, 33–35). IRBIT interacts with the N terminus NBCe1-B AID to relieve autoinhibition by an unknown mechanism (33, 34). NBCe1-B, CFTR and Slc26a6 are regulated by WNK1 and WNK4 kinases that phosphorylate and activate the kinase SPAK (34, 35). Phosphorylation of NBCe1-B S65 by SPAK inhibits the transporter, which is reversed by the phosphatase PP1 (36). Key questions in understanding signaling by Cl^-_{in} are: how Cl^-_{in} sensing by the GXXXP motifs is achieved, how IRBIT modulates regulation by Cl^-_{in}, and whether the kinase/phosphatase pathways interface with Cl^-_{in} and IRBIT to form an integrated signaling pathway. Moreover, it is not clear how interaction of IRBIT with the AID activates the transporters. Herein, we used NBCe1-B as a model to address these questions by identifying the NBCe1-B phosphorylation sites modified by IRBIT, the kinases and phosphatases recruited by IRBIT to control these sites, the effect of specific phosphorylation sites on Cl^-_{in} signaling, and the role of these sites in IRBIT-mediated relief of autoinhibition.

We report that IRBIT exposed the two cryptic N terminal GXXXP motifs and recruited the kinases SPAK and CaMKII or the phosphatases PP1 and Calcineurin (CaN) to NBCe1-B AID. LC-MS/MS analysis of NBCe1-B serine/threonine phosphorylation identified a total of 25 sites. IRBIT-mediated combinatorial dephosphorylation of $S^{232}/S^{233}/S^{235}$ to set three alternative conformers pS^{233}/pS^{235}, pS^{232}/pS^{235} or pS^{232}/pS^{233}. IRBIT also regulated the dephosphorylation of S^{65} and phosphorylation of S^{12}. Notably, S^{232}, S^{233} and S^{235} control NBCe1-B active state and its regulation by IRBIT and Cl^-_{in}. Similar regulation of the active states of (Δ1–95)NBCe1-B and NBCe1-A, which are not regulated by IRBIT, suggesting that the conserved S^{232}, S^{233} and S^{235} determined the active state of these NBC transporters. Functional analysis of NBCe1-B GXXXP motifs showed that SPAK and PP1 acted on S^{65} to regulate Cl^-_{in} sensing by the $^{32}GXXXP^{36}$ motif, while CaN dephosphorylated S^{12} to regulate Cl^-_{in} sensing by the $^{194}GXXXP^{198}$ motif. These findings uncover an intricate mechanism by which Cl^-_{in} signals through IRBIT-mediated recruitment of kinases and phosphatases to regulate key transporters involved in epithelial fluid and electrolyte secretion with implications for epithelial diseases, including cystic fibrosis (CF), pancreatitis and Sjögren's syndrome.

Results

IRBIT interacts with and recruits PP1, CaN, CaMKII and SPAK to NBCe1-B AID:

IRBIT interacts with PP1 (34, 37) and CaMKII (38). We show here that that IRBIT coimmunoprecipitated with PP1, CaMKII and the phosphatase calcineurin (CaN) and the kinase SPAK (Fig. 1a, b). Moreover, IRBIT recruited the phosphatases and kinases to NBCe1-B (Fig. 1c, d) and IRBIT specifically recruited PP1, CaN, SPAK and CaMKII to the N terminus of NBCe1-B(1–95) (Figs. 1e and 1f), which includes the AID of NBCe1-B. The entire NBCe1-B N terminal domain (1–429) also showed IRBIT-mediated interaction of the phosphatases and kinases with the NBCe1-B N terminus.

PP1 and SPAK modulate Cl^-_{in} sensing by the ^{32}GXXXP^{36} motif:

NBCe1-B activity in the presence or absence of IRBIT was measured by recording the HCO_3^--induced current at pipette Cl^- concentration (Cl^-_{in}) of 5 and 140 mM (Fig. 2a). PP1 activates and SPAK inhibits NBCe1-B in an IRBIT-independent manner (34) and IRBIT does not further activate NBCe1-B activated by PP1 (Fig. 2b). NBCe1-B is regulated by Cl^-_{in} and in the absence of IRBIT the inhibition is observed at Cl^-_{in} between 40–140 mM (Fig. 2c). However, when NBCe1-B is activated by IRBIT, inhibition by Cl^-_{in} is observed at Cl^-_{in} between 5–40 mM. Inhibition by the lower Cl^-_{in} depends on IRBIT-mediated exposure of two cryptic Cl^-_{in} sensing ^{32}GXXXP^{36} and ^{194}GXXXP^{198} motifs (23). Mutation of either motif shifts the inhibition by Cl^-_{in} to the right and mutation of both motifs is required to eliminate inhibition by Cl^-_{in} (23).

It is not known whether or how signaling by Cl^-_{in} is regulated by kinases and phosphatases, and the phosphorylation sites involved. To address these questions, we examined the effect of PP1 on inhibition of NBCe1-B by Cl^-_{in}. PP1 activated NBCe1-B in the absence of IRBIT (Fig. 2b), possibly by interacting with a potential NBCe1-B PP1 binding site (^{949}RVHLF^{953}). NBCe1-B activated by PP1 showed low sensitivity for inhibition by Cl^-_{in}, similar to the inhibition observed with NBCe1-B alone (Fig. 2c, Black and green traces), indicating that PP1 does not expose the cryptic GXXXP motifs and does not affect inhibition by Cl^-_{in} when the GXXXP motifs are not exposed by IRBIT. Treating PP1-activated NBCe1-B with IRBIT induced inhibition of NBCe1-B, but only by Cl^-_{in} at 40 and 140 mM (Fig. 2c, red trace). Thus, PP1 eliminated the inhibition of NBCe1-B by 5–20 mM Cl^-_{in} that is observed when NBCe1-B is activated by IRBIT in the absence of PP1 (Fig. 2c, blue trace). This indicates that PP1 acting on IRBIT-activated NBCe1-B must have affected Cl^-_{in} sensing by one of the GXXXP motifs. To identify the GXXXP motif affected by PP1, the effect of PP1 on NBCe1-B(^{32}GP/AA^{36}) and NBCe1-B(^{195}GP/AA^{199}) activity was tested (Fig. 2d). PP1 did not affect the inhibition of NBCe1-B(^{32}GP/AA^{36}) by 140 mM Cl^-_{in} (in which the ^{194}GXXXP^{198} motif is available for Cl^- sensing, as illustrated in the models), while treatment of NBCe1-B(^{195}GP/AA^{199}) (in which the ^{32}GXXXP^{36} motif is available) with PP1 eliminated inhibition by Cl^-_{in}, indicating that PP1 affect Cl^-_{in} sensing by the available ^{32}GXXXP^{36} motif and not by the ^{194}GXXXP^{198} motif (see models).

SPAK phosphorylates NBCe1-B S^{65} to inhibit NBCe1-B activity, an activity antagonized by PP1 (36), suggesting that phosphorylation of S^{65} by SPAK may affect the same GXXXP motif affected by PP1. Accordingly, PP1 did not affected the inhibition of NBCe1-B(S^{65}) by 140 mM Cl^-_{in}, (Fig. S1). To directly examine this prediction, we tested whether dominant negative (DN) SPAK and the S^{65}A mutant had the same effect as PP1 on inhibition of NBCe1-B by Cl^-_{in}. IRBIT-activated NBCe1-B treated with DN-SPAK (Fig. 3a) and IRBIT-activated NBCe1-B(S^{65}A) were not inhibited by low Cl^-_{in}, while the phosphomimetic NBCe1-B(S^{65}E) mutant showed the expected strong inhibition by 10–40 mM Cl^-_{in} (Fig. 3c). When tested on NBCe1-B(^{32}GP/AA^{36}) and NBCe1-B(^{194}GP/AA^{198}), both DN-SPAK (Fig. 3b) and NBCe1-B(S^{65}A) mutation (Fig. 3d) eliminated Cl^- sensing by the ^{32}GXXXP^{36} motif. As illustrated in the GXXXP models (Figs. 3b–d), because DN-SPAK affected Cl^-_{in} sensing by NBCe1-B(^{194}GP/AA^{198}) but not by NBCe1-B(^{32}GP/AA^{36}) mutants, SPAK acts on S^{65} to modulate Cl^-_{in} sensing by the ^{32}GXXXP^{36} motif, similar to PP1.

CaN and CaMKII modulate Cl^-_{in} sensing by the ^{194}GXXXP^{198} motif:

IRBIT recruited CaN and CaMKII to NBCe1-B (Fig. 1). In oocytes constitutively active (CA) CaN (Fig. 4a) and CaMKII (Fig. 4b) had no effect on NBCe1-B activity when expressed without IRBIT. However, in the presence of low levels of IRBIT CA-CaN markedly activated NBCe1-B to the level observed with maximal stimulation with IRBIT (Fig. 4a). IRBIT ^{271}LxVP^{274} is a CaN-interacting motif and the IRBIT$^{LCVP/AAAA}$ mutant failed to activate NBCe1-B when expressed with or without CA-CaN (Fig. 4a). CaMKII inhibited NBCe1-B activated by intermediate concentrations of IRBIT (Fig. 4b). Thus, these findings suggest that the CaN/CaMKII pair reciprocally regulates the activity of NBCe1-B.

The findings with CaN in oocytes were extended to HEK cells to examine the effect of CaN on signaling by Cl^-_{in}. CaN modestly activated NBCe1-B in the absence of IRBIT (Fig. 4c). In the presence of IRBIT CaN altered the inhibition by Cl^-_{in}, shifting the inhibition to higher Cl^-_{in} (Fig. 4c, 4d). Interestingly, use of the GXXXP mutants showed that CaN influenced Cl^-_{in} sensing by the ^{194}GXXXP^{198} motif (Fig. 4e), rather than the ^{32}GXXXP^{36} motif affected by PP1. Accordingly, treating IRBIT-activated NBCe1-B with both PP1 and CaN eliminated inhibition by Cl^-_{in} (Fig. 4c, d). Hence, the two GXXXP motifs appears to cooperate in determining regulation by Cl^-_{in} with elimination of the effect of each motif similarly reduces the affinity for Cl^-_{in} and only when both motifs are not available for Cl^-_{in} sensing does inhibition by Cl^-_{in} prevented (see models in Figs. 4c, d). Similar studies with CaMKII expressed in HEK cells were not possible since CaMKII modestly activated NBCe1-B and altered inhibition by Cl^-_n (Supplementary Fig. S2a, b). It is not clear why CaMKII acted so differently in oocytes and mammalian cells. However, this is not without precedent. Regulation of NBCe1-B by PP1 is quite different in HEK cells (34) and oocytes (39).

Identifying the IRBIT-regulated NBCe1-B phosphorylation sites:

To identify NBCe1-B phosphorylation sites affected by IRBIT, we defined the NBCe1-B phosphorylation sites in the presence and absence of IRBIT using LC-MS/MS-based phosphoproteomics (40) and identified 20 phosphorylation sites at the long N terminus domain and 5 sites in the C terminus (Fig. S3a). All previously reported phosphorylation sites, T^{49}, S^{1026} (41) and S^{65} (36) were identified by our phosphoproteomic analysis. Similar analysis in the presence of IRBIT revealed that IRBIT caused phosphorylation of S^{12} (red in Fig. S3a) and dephosphorylation of S^{232}, S^{233} and S^{235} (magenta in Fig. S3a). In the case of S^{12}, only one phosphorylated peptide was found (Fig. S3b). For S^{232}, S^{233} and S^{235}, two separate phosphorylated peptides were identified in this region (Fig. S3c). For peptides in which S^{232} and S^{233} were phosphorylated, S^{235} was not phosphorylated. For peptides in which S^{235} was phosphorylated, either S^{232} or S^{233} was phosphorylated, but not both. These findings indicate that IRBIT has a combinatorial effect on dephosphorylation of these sites, with the conformations NBCe1-B(pS^{232}/pS^{233}), NBCe1-B(pS^{232}/pS^{235}) and NBCe1-B(pS^{233}/pS^{235}), with p denoting phosphorylation. Localization of the phosphorylation sites in the N terminus of NBCe1-B, and the orientation of these sites with respect to the GXXXP motifs and the ion transporting sector of NBCe1-B is shown in the structural model of NBCe1-B (Fig. S4). All the three phosphorylation sites are conserved in the kidney specific isoform NBCe1-A and the first phosphorylation site (equivalent to NBCe1-B(S^{232}) is conserved in all members of the NBC family (Fig. S5).

NBCe1-B S^{12} mediates the effect of CaN on Cl^- sensing by the ^{194}GXXXP^{198} motif:

Using nonphosphorylatable [NBCe1-B(S^{12}A)] or a phosphomimetic [NBCe1-B(S^{12}D)] mutants showed that mutating S^{12} did not affect the surface expression of NBCe1-B or its interaction with IRBIT (Fig. 5a). At 5 mM $Cl^-_{in,}$ NBCe1-B(S^{12}A) had no effect on NBCe1-B activity in the absence of IRBIT (Fig. 5b) and a small effect in the presence or absence of IRBIT (Fig. 5c), while NBCe1-B(S^{12}D) increased NBCe1-B activity in the presence of absence of IRBIT by about 60% (Fig. 5b, c). By contrast, NBCe1-B(S^{12}D) had no effect on the inhibition of NBCe1-B activity by Cl^-_{in}, while NBCe1-B(S^{12}A) shifted the inhibition by Cl^-_{in} to the high mM range (Fig. 5c, d). PP1 and DN-SPAK reduced inhibition of NBCe1-B(S^{12}A) by 140 Cl^-_{in} while CaN did not (Fig. 5e and associated models). These findings suggest that S^{12} regulates Cl^-_{in} sensing by the ^{194}GXXXP^{198} motif and pS^{12} is dephosphorylated by CaN. Accordingly, the S^{12}A mutation eliminated inhibition by 140 mM Cl^- of the NBCe1-B(^{32}GP/AA^{36}) mutant (in which the ^{194}GXXXP^{198} motif is available), but not of the NBCe1-B(^{194}GP/AA^{198}) mutant (in which the ^{32}GXXXP^{36} motif is available) (Fig. 5e and associated models).

S^{232}, S^{233} and S^{235} regulate NBCe1-B active state and activation by IRBIT:

Since IRBIT caused combinatorial dephosphorylation of S^{232}, S^{233} and S^{235}, the role of each serine residue was studied by mutating them individually and in combination to alanine to prevent phosphorylation at these sites, and to aspartates as phosphomimetics. The combined and individual mutations had no obvious effect on NBCe1-B total and surface expression or interaction with IRBIT (Fig. 6a, b).

However, mutating serines 232/233/235 to alanines [NBCe1-B(AAA)] resulted in fully activated NBCe1-B that was not activated further by IRBIT (Fig. 6c). On the other hand, mutation of all serines to aspartates [NBCe1-B(DDD)] nearly completely inhibited NBCe1-B activity, and it could not be rescued or activated by IRBIT. To further confirm that NBCe1-B(AAA) and NBCe1-B(DDD) function was independent of IRBIT, we mutated three residues in NBCe1-B(Δ1–95), which lacks the autoinhibitory IRBIT-binding domain (36, 42). The AAA mutation also maximized the activity of NBCe1-B(Δ1–95), while the DDD mutation markedly inhibited NBCe1-B(Δ1–95) activity (Fig. 6c). In addition, we mutated the three residues in NBCe1-A, which functions independently of IRBIT. NBCe1-A activity was increased by the AAA mutation and inhibited by the DDD mutation (Fig. 6c).

To further analyze the role of S^{232}, S^{233} and S^{235}, we measured the activity of the individual mutants at 5 mM Cl^-_{in} (Fig. 6d). Mutation of S^{232}A (conformer A, in which pS^{233}/pS^{235} are phosphorylated) resulted in activation of NBCe1-B with minimal further activation by IRBIT. Mutation of S^{233}A (conformer B, in which pS^{232}/pS^{235} are phosphorylated) did not activate NBCe1-B, which was then fully activated by IRBIT. Mutation of S^{235}A (conformer C, in which pS^{232}/pS^{233} are phosphorylated) resulted in activation of NBCe1-B, but in this case IRBIT markedly increased transporter activity (Fig. 6d). S^{232}D and S^{233}D minimally affect basal NBCe1-B activity but eliminated activation by IRBIT. By contrast, S^{235}D significantly inhibited basal NBCe1-B activity, but the residual activity was activated by IRBIT to similar extent of activation of wild-type NBCe1-B (Fig. 6c and 6d). Inhibition of NBCe1-B by the aspartate mutants was independent of IRBIT since similar inhibition was

observed when these residues were mutated in NBCe1-B(Δ1–95) (Fig. S6b). The inhibition was independent of total or surface expression of NBCe1-B(Δ1–95) (Fig. S6a).

The decoupling of NBCe1-B activity from IRBIT caused by mutating S^{232} raised the question of the role played by S^{232} and this region of NBCe1-B in activation of the cotransporter. We addressed this question by mutating S^{232} to various residues. All mutations tested were tolerated and did not affect NBCe1-B total and surface expression or interaction with IRBIT (Fig. S7a). Measurement of NBCe1-B activity showed that adding a negative charge at S^{232} (Asp and Glu) resulted in inhibition of transport and loss (S^{232}D) or reduced (S^{232}E) activation by IRBIT (Fig. S7b). Replacing S^{232} with residues that can be phosphorylated by kinases (Thr and Tyr) did not restore the wild-type phenotype but resulted in a phenotype similar to S^{232}A. A positive charge (Lys), a polar residue (Gln), a small residue (Leu) and a bulky (Trp) hydrophobic residue, all resulted in phenotype similar to S^{232}A. Residues that introduce kinks (Gly and Pro) were less effective in activating NBCe1-B but resulted in maximal activation by IRBIT. These findings suggest that S^{232} is in a conformation-sensitive sector of the protein, and that dephosphorylation by IRBIT stabilizes an active conformation. Conservation of the equivalent S^{232} in NBCe2-C (Fig. S5), provides further evidence in support of a critical role of this serine since the mutant NBCe2-C(S^{236}D) reduced the activity (Fig. S8). Together, the findings suggest that the phosphorylation state of S^{232} determines whether NBCe1-B is in an active or inactive conformation and by binding to the AID, IRBIT activates NBCe1-B by dephosphorylating this site.

S^{232} but not S^{235} modulates Cl^-_{in} sensing:

Current measurement of NBCe1-B(AAA) showed that activation of the current did not affect the reversal potential, and thus transporter ionic selectivity (Fig. 7a). However, the S^{232}, S^{233} and S^{235} mutants affected signaling by Cl^-_{in}. NBCe1-B(AAA) and NBCe1-B(S^{232}A) are not inhibited by Cl^-_{in} in the presence or absence of IRBIT (Fig. 7b). Hence, when S^{233} and S^{235} are phosphorylated (in the S^{232}A mutant), NBCe1-B is fully active with the Cl^-_{in} sensing motifs occluded within the N terminus domain. In the presence of IRBIT, S^{233}A was inhibited by 40 and 140 mM Cl^-_{in} (Fig. 7c). The actual and normalized currents of NBCe1-B(S^{235}A) (Fig. 7d) showed that in the absence of IRBIT the increased activity of NBCe1-B(S^{235}A) was inhibited by 140 mM, but not by 40 mM Cl^-_{in}, similar to the inhibition of NBCe1-B alone. IRBIT maximized the activity of NBCe1-B(S^{235}A) and at the same time exposed inhibition by Cl^-_{in} (Fig. 7d). The inhibition followed a shallower curve than that observed with NBCe1-B activated by transfection with 1 μg/ml IRBIT cDNA (for example Figs. 2c, 5c). We reason that this may be due to the maximal activity observed with NBCe1-B(S^{235}A) activated by IRBIT. Indeed, transfecting the cells with wild-type NBCe1-B and very high IRBIT resulted in a Cl^-_{in} inhibitory curve similar to that observed with NBCe1-B(S^{235}A) stimulated by IRBIT (Fig. 7d). These findings suggest that inhibition by Cl^-_{in} depends on the extent of activation of NBCe1-B by IRBIT and that when pS^{232} and pS^{233} are phosphorylated (as in the S^{235}A mutant) NBCe1-B has higher basal activity. Binding of IRBIT to this NBCe1-B form fully activate it and exposes its cryptic GXXXP Clin sensing motifs.

Discussion

Cl^- is the major anion and important osmolyte in most living cells and has a prominent role in cellular homeostasis by affecting cytoplasmic ionic composition, pH, cell volume and the membrane potential. These roles are related mostly to the transport function of Cl^-. Another form of regulation by Cl^- involves direct interaction of Cl^- with the transporters. For example, Cl^-_{in} regulates the mammalian neurotransmitter transporters (43, 44), the anion exchanger AE1 (45) and the SLC26 transporters Slc26a5 (also known as Prestin) (46), Slc26a1 and Slc26a2 (26, 47). Cl^- is sensed by a GXXXP motif in Slc26a2 (26). The family of cotransporters and exchangers has one or more GXXXP motifs and Cl^-_{in} sensing by the GXXXP motifs inhibits the transporters at Cl^-_{in} between 5–40 mM (23), well within the physiological range of Cl^-_{in} changes. In the present studies, we used regulation of NBCe1-B by Cl^-_{in} as a model to understand how Cl^- regulates the transporters and how Cl^- sensing by the transporters is regulated.

At the basal state NBCe1-B has low activity due to inhibition by its AID, a conformation in which the two Cl^-_{in} sensing GXXXP motifs are not accessible. In the resting state IRBIT is sequestered by binding to IP_3 receptors (35, 48). Upon cell stimulation IRBIT is released from the IP_3Rs and interacts with and activates NBCe1-B and other epithelial transporters (35), and exposes their Cl^- sensing motifs (23).

Here, we found that IRBIT controls autoinhibition by a combinatorial dephosphorylation of S^{232}, S^{233} and S^{235} to induce various NBCe1-B conformations, each of which has different properties (Figure 7e). S^{232}, S^{233} and S^{235} appear to reside in a conformation sensitive site in NBCe1-B. S^{232} is conserved in all members of the NBC family and its dephosphorylation results in conformation pS^{233}/p^{S235} (conformation A in Fig. 7e). This conformation is active independently of autoinhibition and Cl^-_{in}-dependent inhibition, as demonstrated by the findings that mutation of S^{232} to any residue, except for the phosphomimetics Asp and Glu, resulted in partial or full activation of NBCe1-B independent of IRBIT, and that similar activation was observed with the constitutively active NBCe1-B mutant lacking the AID (NBCe1-B(Δ1–95)) and NBCe1-A (Fig. 6c, d and S7b). Moreover, mutation of S^{232} to Asp or Glu strongly inhibited NBCe1-B, NBCe1-B(Δ1–95) and NBCe1-A without affecting the interaction with IRBIT or surface expression (Fig. 6a–d, S6a, b and S7a, b). Together, these findings suggest that S^{232} controls the communication between the large cytoplasmic N terminus and the transmembrane sector of NBCe1-B to affect opening of the permeation pathway.

The second IRBIT-induced NBCe1-B conformation is phosphorylated S^{232}/S^{235} (conformation B, pS^{232}/pS^{235} in Fig. 7e). Conformation B properties are similar to wild-type NBCe1-B: it is inactive in the absence of IRBIT with cryptic Cl^-_{in} sensing motifs. IRBIT activates NBCe1-B(pS^{232}/pS^{235}) and exposes the Cl^-_{in} sensing motifs that are, in turn, regulated by the PP1/SPAK and CaN/CaMKII affecting Cl^-_{in} sensing by the respective GXXXP motifs. The third IRBIT-induced NBCe1-B conformation is phosphorylated S^{232}/S^{233} (conformation C, pS^{232}/pS^{233} in Fig. 7e). The properties of conformation C are intermediate between those of conformations A and B. In conformation C basal NBCe1-B activity is increased independent of the AID, as suggested by the low sensitivity to Cl^-_{in}.

However, IRBIT further activates conformer C and exposes the cryptic GXXXP motifs that are regulated by PP1/SPAK and CaN/CaMKII. Hence, regulation by IRBIT is more complicated than originally thought, with IRBIT able to tune NBCe1-B activity to match physiological demands.

Cl^-_{in} sensing is conferred by two GXXXP motifs that are selectively affected by SPAK/PP1 and CaN/CaMKII mediated phosphorylation of S^{65} and S^{12}, respectively. The two GXXXP motifs appears to cooperate to determine regulation by the same or associated Cl^-_{in} sites. This is suggested by the findings that elimination of the effect of any of the motifs, either by SPAK/PP1 and CaMKII/CaN or by mutations, similarly reduce the affinity for inhibition by Cl^-_{in} to shift the inhibition to a higher Cl^-_{in}. Only when both motifs are not available for Cl^-_{in} sensing does inhibition by Cl^-_{in} is eliminated.

The present and previous work suggest that the kinase/phosphatase pathways affect NBCe1-B beyond regulation of Cl^-_{in} sensing. Hence, SPAK controls transporter activity by two mechanisms, modifying transporter surface expression and sensing of Cl^- by the ^{32}GXXXP^{36} motif. In the absence of IRBIT NBCe1-B activity is low, and SPAK inhibits NBCe1-B activity by reducing surface expression (36). Although IRBIT antagonizes the effect of SPAK on NBCe1-B surface expression (34), SPAK can still phosphorylate S^{65} in the presence of IRBIT, which affects Cl^-_{in}-mediated regulation of NBCe1-B at the ^{32}GXXXP^{36} motif. Cl^- may regulate SPAK activity directly or indirectly through WNK4 (32) to inhibit SPAK activity. However, it is not clear what effect Cl^- between 5–20 mM has on SPAK activity, which are the concentrations at which SPAK affects Cl^- regulation of NBCe1-B.

Our findings have broader physiological implications by demonstrating the use of multiple phosphorylation sites to fine-tune transporter activity to meet variable demands. A good example is fluid and HCO_3^- secretion by the stimulated pancreatic and salivary ducts, which secrete fluid containing 140 mM HCO_3^- (30). As fluid and HCO_3^- secretion progresses from the intercalated to the intralobular, interlobular and the main ducts, secretion occurs at increased luminal HCO_3^- concentration and thus requires enhanced basolateral HCO_3^- influx. The ducts likely use combinations of phosphorylation sites to tune HCO_3^- influx by NBCe1-B in various portions of the duct. It is likely that in the intercalated duct NBCe1-B S^{65}, S^{232} and S^{235} are phosphorylated and S^{12} and S^{233} are dephosphorylated and together with the high Cl^-_{in} maintain low NBCe1-B activity that is sufficient for the initial HCO_3^- secretion. In the main duct S^{12} is phosphorylated, S^{65} and S^{232} are dephosphorylated and together with the low Cl^-_{in} maximize NBCe1-B activity and basolateral HCO_3^- uptake to support HCO_3^- secretion into a lumen that already contains 120 mM HCO_3^-. Combinations of these extremes operate along the ducts to tune NBCe1-B activity and ductal HCO_3^- secretion. Thus phosphorylation/dephosphorylation of S^{12}, S^{65}, S^{232}, S^{233}, S^{235} together with changes in Cl^-_{in} between 5–40 mM function as a rheostat to tune NBCe1-B activity and NBCe1-B-dependent functions.

Materials and Methods

Plasmids:

The p3xFLAG-CMV-7.1/IRBIT, pCMV-HA-IRBIT, pEGFP-C1/NBCe1-B, pEGFP-C1/NBCe2-C, pCDNA 3.1+/NBCe1-A constructs were described previously(36). pCDNA3-Flag calcineurin is a gift from Drs. Rhonda Bassel-Duby and Eric Olson (University of Texas Southwestern Medical Center), pCDNA-CaMKαII is a gift from Dr. Leta Nutt (St. Jude Children's Research Hospital, Memphis), and pCDNA3/mPP1 was a gift from Dr. Eric Delpire (Vanderbilt University Medical Center, Nashville). The cDNA encoding SPAK (a gift from Melanie Cobb, University of Texas Southwestern Medical Center) was excised from the original vectors and transferred to pCMV-myc. Point mutations were generated by site-directed mutagenesis with a Quick light chain mutagenesis kit (Agilent), using primers to change specific regions. All constructs were verified by sequencing of the entire open reading frames.

Surface Expression and Co-immunoprecipitation:

Biotinylation of surface proteins was performed by incubating transfected HEK cells with 0.5 mg/mL EZ-LINK Sulfo-NHS-LC-biotin (Thermo Scientific) for 30 min on ice. The cells were then treated with 100 mM glycine for 10 min to terminate the biotinylation reaction, washed with PBS, and lysed with ice-cold lysis buffer (10 mM $NaPO_4^{3-}$, 137 mM NaCl, 2.7 mM KCl, 50 mM NaF, 1% Triton X-100, and protease inhibitor cocktail (Roche)) for 20min on ice. After brief sonication, lysates were collected by centrifugation. Biotinylated proteins were captured with avidin beads (Thermo Scientific) by incubation for 1 h at 4°C. The precipitated proteins were analyzed by SDS/PAGE. Co-immunoprecipitation was performed by incubation overnight of 300 μg of proteins with corresponding antibodies for each protein: NBCe1-B (anti-GFP, Invitrogen A11122), IRBIT (anti-HA, Cell signaling 2367S), Calcineurin (anti-FLAG, Sigma F3165) anti-MYC, (Cell Signaling 2276S), CAMKIIα (Santa Cruz 13141). The next day, Protein G Sepharose beads (GEhealthcare) are added and incubated for 2 h at 4°C. Beads were collected by centrifugation and washed 3 times with lysis buffer, and proteins were recovered by 30 min heating at 56°C in SDS sample buffer. Proteins were subjected to SDS/PAGE and the blots probed for the indicated proteins.

Pull down:

The N-terminus 95 (1–95) first amino acids and 429 amino acids (1–429) of NBCe1-B were subcloned in the pQE-TriSystem His-Strep vector (Qiagen). The final plasmid constructs were transformed into E. coli strain Rosetta (DE3) competent cells. Colonies were amplified in 10 mL of LB media containing 100 ug/mL ampicillin and incubated at 37°C overnight under shaking (250 rpm). Aliquots were then used to inoculate larger volume cultures. Protein expression was induced to OD600=0.6 by addition of isopropyl-beta-D-thiogalactopyranoside (IPTG) to a final concentration of 0.1 mM. His-tagged proteins were extracted by lysis and sonication and extracts were clarified by centrifugation at 20,000 g for 20 min. Fusion proteins were purified with Ni-NTA superflow beads (Qiagen). Purity of proteins was better than 80%, as determined by Coomassie Blue staining. HEK cell lysates expressing NBCe1-B and the kinases or phosphatases as indicated were incubated with Strep-tagged fusion proteins bound to the beads for 4h at 4 °C. The beads were washed with

lysis buffer and proteins were released by incubation in SDS sample buffer at 56°C for 20min and analyzed by SDS-PAGE and western blotting.

Determination of NBCe1-B phosphorylation site:

Cells expression NBCe1-B alone or NBCe1-B and IRBIT were lysed with 8M urea and sonicated. The cell lysates were reduced by addition of 20 mM dithiothreitol, alkylated with 40 mM iodoacetamide, and diluted with 20 mM triethylammonium bicarbonate (TEAB) buffer (pH 8.5) to reduce urea to 1M. The lysates were then digested with trypsin (Promega, enzyme) at a lysate/trypsin ratio of 1:20. Peptides were desalted using hydrophilic-lipophilic-balanced extraction cartridges (Oasis), and then subjected to phospho-peptide enrichment using either Fe-NTA or TiO2 columns per manufacture's protocol (ThermoFisher). The enriched peptides were desalted using graphite columns, vacuum-dried and stored at −80°C. Peptides were re-suspended with 0.1% formic acid for mass spectrometry (Orbitrap Fusion ETD mass spectrometer, ThermoFisher) analysis. Mass Spec spectra were analyzed using Proteome Discoverer 1.4 software (ThermoFisher). Peptide-spectra matching (false discovery rate <0.01, peptide rank = 1) was analyzed by both Mascot and SequestHT software, and the human Swiss-prot (Nov. 18, 2016) protein database. The probabilities of the phosphorylation site localizations were calculated using the phosphoRS 3.1 Module within Proteome Discoverer 1.4.

Current measurement in HEK-293 cells:

The effect of Cl^-_{in} on current mediated by NBCe1-B, NBCe1-A, and NBCe2-C activity was analyzed in transiently transfected HEK-293 cells using whole-cell current recording at room temperature, exactly as detailed previously(23), and varying pipette Cl^- concentration between 5 and 140 mM. Patch pipettes had a resistance of 5–7 MΩ when filled with CsCl-based pipette solution. The cell capacitance was between 10–18 pF. The pipette solutions contained (in mM): 2 $MgSO_4$, 1 ATP, 0.5 EGTA, 10 Hepes and a mixture of CsCl and Cs-gluconate to yield Cl^- concentrations of 5, 10, 20, 30, 40, and 140 mM. pH was adjusted to 7.3 with CsOH. The Hepes-buffered bath solution contained (in mM): 140 NaCl, 5 KCl, 1 $MgCl_2$, 1 $CaCl_2$, 10 glucose, 10 Hepes (pH 7.4 with NaOH). The HCO_3^--buffered solution was prepared by replacing 25 mM NaCl with equimolar amount of $NaHCO_3$, and the solution was equilibrated with 5% CO_2/95% O_2. The current was recorded by 400-ms rapid alteration of membrane potential (RAMPs) from −60 to +60 mV every 2 s from a holding potential of 0 mV. Before current recording the junction potential at each pipetted solution Cl^- concentration was offset to 0 using the Axopatch 200B amplifier. The current recorded at +60 mV was used to calculate current density as pA/pF. Axopatch 200B patch-clamp amplifier, Digidata −1440A, and pClamp 10 software (Molecular Devices) were used for data acquisition and analysis. The currents were filtered at 1 kHz and sampled at 10 kHz.

Preparation of cRNA:

The human NBCe1-B/pcDNA3.1 and human IRBIT/pcDNA3.1 plasmids were used as templates for preparation of the corresponding cRNAs. DNA was linearized with SmaI (NBCe1-B) or Xba1 (IRBIT) (New England Biolabs, Ipswich, MA). cRNA was then transcribed *in vitro* using a T7 PNA polymerase kit (mMessage mMashine T7 Kit; Ambion

Inc., Austin, TX). cRNA was purified by phenol/chloroform extraction, precipitated with isopropanol and then dissolved in Nuclease-Free Water (Ambion Inc., Austin, TX).

Preparation and injection of Xenopus oocytes:

Oocytes were obtained by partial ovariectomy of female *Xenopus Laevis* (Xenopus Express, Beverly Hills, FL), anesthetized with 2.0 g/l methanesulfonate salt of 3-aminobenzoic acid ethyl ester (Sigma, St. Louis, MO). Follicle cells were removed in OR-2 Ca^{2+}-free medium (in mM 82.5 NaCl, 2.4 KCl, 1.0 $MgCl_2$, 5.0 HEPES-Na, pH 7.5) with addition of 1 mg/ml collagenase B (Boehringer Mannheim, Indianapolis, IN). Defolliculated oocytes were washed 4 to 5 times with Ca^{2+}-free OR-2. Healthy oocytes in stages V to VI were collected under a microscope and maintained at 18°C overnight in ND96 solution (in mM, 96.0 NaCl, 2.0 KCl, 1.8 $CaCl_2$, 1.0 $MgCl_2$, 2.5 sodium pyruvate, 5.0 HEPES-Na, pH 7.5, 100 μg/ml streptomycin, and 100 U/ml penicillin). Oocytes were injected with indicated amount of cRNA in a final volume of 50 nl using a Nanoliter 2000 injector (World Precision Instruments, Inc., Sarasota, FL). Oocytes were incubated at 18°C in ND96 solution with pyruvate and antibiotics. The medium was changed every day, and oocytes were tested 48–96 hr after cRNA injection.

Measurement of membrane current and voltage in oocytes:

Electrophysiological recordings were performed at room temperature with two-electrode voltage-clamp or current-clamp using an OC-725C Oocyte Clamp System (Warner Instrument Corp., Hamden, CT). The microelectrodes were filled with 3M KCl (resistance 0.5–2 MΩ). During recording, the oocytes were superfused with ND96 solution. The Cl^- and HCO_3^--containing solutions were of (in mM) 71.0 NaCl, 25.0 NaCl or $NaHCO_3$, 2.0 KCl, 1.8 $CaCl_2$, 1.0 $MgCl_2$, 5.0 HEPES-Na, pH 7.5). Solutions were constantly gassed with 5% CO_2/95% O_2. Current and voltage were digitized via a Digidata 1322A A/D converter (Axon Instrument, Foster City, CA) and analyzed using Clampex 8.1 system.

Structure Prediction and Protein Modeling:

A segment of mouse NBCe1-B, consisting of 1,000 amino acids (NP_061230.2), was submitted to both ROBETTA and hhPRED. The ROBETTA software generated different models for 3 segments of the submitted sequence. No homology was identified for segment 1–106. Segment 107–413 was homologous to Putative Substrate Access Tunnel in the Cytosolic Domain of Human Anion Exchanger 1 (Protein Data Bank ID 4KY9) which is similar to human erythrocyte band 3 cytoplasmic domain (Protein Data Bank ID 1HYN) that we previously used to predict NBCe1-B N-terminus (23) and the same structure is used here. The transmembrane segment spanning residues 414–1000 was found to be homologous to the structure of the anion exchanger domain of human erythrocyte Band 3 (Protein Data Bank ID 4YZF). The highest TMD homology score provided by the hhPRED software was for the Electrogenic sodium bicarbonate cotransporter 1, NBCe1 (PDB_ID 6CAA). (Probability: 100, E-value: 2.5e-164, SS:108.9, Cols:1003). NBCe1 TMD structure was recently solved by CryoEM (49). The final model was generated using PyMOL with the TMD in blue and intracellular domains as predicted by hhPRED and ROBETTA, respectively. The orientation of the N terminus with respect to the TMD is not known with certainty and may not be accurate. However, the overall structure is reasonable since the

software identified AE1 as the best template that like NBCe1-B is a member of the SLC4 transporters superfamily. In addition, we have previously predicted the structure of NBCe1-B to be similar to the crystal structure of UraA (23), which is highly similar to the crystal structure of AE1. This indicates that the software predicted the same structure twice and independently based on several similar, yet different structures.

Statistics:

Results are given as mean ± SEM, and significance was analyzed by Student *t* test or Two-Way-ANOVA, as appropriate.

Supplementary Material

Refer to Web version on PubMed Central for supplementary material.

Acknowledgments:

We thank Dr. Daniella M. Schwartz (NIAMS) for fruitful discussion and suggestions and Drs. Ronda Bassel-Duby and Eric Olson for providing the Ca^{2}+-$CaNR^{392X}$ plasmid.

Funding:

These studies were funded by Division of Intramural Research National Institute of Dental and Craniofacial Research (NIDCR), intramural grants DE000735-07 (to SM), the National Heart, Lung, and Blood Institute (project ZIA-HL001285 and ZIA-HL006129, to MAK). The NHLBI Proteomics Core Facility (M. Gucek, Director) was utilized. By fellowships from the Nakatomi, Sumitomo Life Welfare, Culture and the Mochida Memorial Foundations and JSPS KAKENHI Grant Number JP16K18992 to OY, and by the Mitsukoshi Health and Welfare Foundation to AY. By Grant No. 2015003 from the United States-Israel Binational Science Foundation (BSF) to SM and EO, ISF grants 271/16 and 2164/16 by the ISRAEL SCIENCE FOUNDATION to EO, by a Basic Science Research Program through the National Research Foundation of Korea (NRF-2016R1A5A2008630 to DMS).

References and Notes

1. Eladari D, Chambrey R, Picard N, Hadchouel J, Electroneutral absorption of NaCl by the aldosterone-sensitive distal nephron: implication for normal electrolytes homeostasis and blood pressure regulation. Cell Mol Life Sci 71, 2879–2895 (2014); published online EpubAug (10.1007/s00018-014-1585-4). [PubMed: 24556999]
2. Miyazaki H, Shiozaki A, Niisato N, Marunaka Y, Physiological significance of hypotonicity-induced regulatory volume decrease: reduction in intracellular Cl− concentration acting as an intracellular signaling. American journal of physiology. Renal physiology 292, F1411–1417 (2007); published online EpubMay (10.1152/ajprenal.00244.2006). [PubMed: 17244897]
3. Zhao H, Muallem S, Na+, K+, and Cl− transport in resting pancreatic acinar cells. The Journal of general physiology 106, 1225–1242 (1995); published online EpubDec ([PubMed: 8786358]
4. Ishiguro H, Naruse S, Kitagawa M, Mabuchi T, Kondo T, Hayakawa T, Case RM, Steward MC, Chloride transport in microperfused interlobular ducts isolated from guinea-pig pancreas. The Journal of physiology 539, 175–189 (2002); published online EpubFeb 15 [PubMed: 11850511]
5. Glykys J, Dzhala V, Egawa K, Balena T, Saponjian Y, Kuchibhotla KV, Bacskai BJ, Kahle KT, Zeuthen T, Staley KJ, Local impermeant anions establish the neuronal chloride concentration. Science 343, 670–675 (2014); published online EpubFeb 07 (10.1126/science.1245423). [PubMed: 24503855]
6. Yamada J, Okabe A, Toyoda H, Kilb W, Luhmann HJ, Fukuda A, Cl− uptake promoting depolarizing GABA actions in immature rat neocortical neurones is mediated by NKCC1. The Journal of physiology 557, 829–841 (2004); published online EpubJun 15 (10.1113/jphysiol.2004.062471). [PubMed: 15090604]

7. Lee MG, Ohana E, Park HW, Yang D, Muallem S, Molecular mechanism of pancreatic and salivary gland fluid and HCO3 secretion. Physiological reviews 92, 39–74 (2012); published online EpubJan (10.1152/physrev.00011.2011). [PubMed: 22298651]
8. Stauber T, Weinert S, Jentsch TJ, Cell biology and physiology of CLC chloride channels and transporters. Comprehensive Physiology 2, 1701–1744 (2012); published online EpubJul (10.1002/cphy.c110038). [PubMed: 23723021]
9. Oh U, Jung J, Cellular functions of TMEM16/anoctamin. Pflugers Archiv : European journal of physiology 468, 443–453 (2016); published online EpubMar (10.1007/s00424-016-1790-0). [PubMed: 26811235]
10. Gagnon KB, Delpire E, Molecular physiology of SPAK and OSR1: two Ste20-related protein kinases regulating ion transport. Physiological reviews 92, 1577–1617 (2012); published online EpubOct (10.1152/physrev.00009.2012). [PubMed: 23073627]
11. Romero MF, Chen AP, Parker MD, Boron WF, The SLC4 family of bicarbonate (HCO(3)(−)) transporters. Molecular aspects of medicine 34, 159–182 (2013); published online EpubApr-Jun (10.1016/j.mam.2012.10.008). [PubMed: 23506864]
12. Ohana E, Yang D, Shcheynikov N, Muallem S, Diverse transport modes by the solute carrier 26 family of anion transporters. The Journal of physiology 587, 2179–2185 (2009); published online EpubMay 15 (10.1113/jphysiol.2008.164863). [PubMed: 19015189]
13. Parker MD, Boron WF, The divergence, actions, roles, and relatives of sodium-coupled bicarbonate transporters. Physiological reviews 93, 803–959 (2013); published online EpubApr (10.1152/physrev.00023.2012). [PubMed: 23589833]
14. Kunzelmann K, Tian Y, Martins JR, Faria D, Kongsuphol P, Ousingsawat J, Thevenod F, Roussa E, Rock J, Schreiber R, Anoctamins. Pflugers Archiv : European journal of physiology 462, 195–208 (2011); published online EpubAug (10.1007/s00424-011-0975-9). [PubMed: 21607626]
15. Piala AT, Moon TM, Akella R, He H, Cobb MH, Goldsmith EJ, Chloride sensing by WNK1 involves inhibition of autophosphorylation. Science signaling 7, ra41 (2014); published online EpubMay 06 (10.1126/scisignal.2005050). [PubMed: 24803536]
16. Terker AS, Zhang C, Erspamer KJ, Gamba G, Yang CL, Ellison DH, Unique chloride-sensing properties of WNK4 permit the distal nephron to modulate potassium homeostasis. Kidney international 89, 127–134 (2016); published online EpubJan (10.1038/ki.2015.289). [PubMed: 26422504]
17. Pacheco-Alvarez D, Gamba G, WNK3 is a putative chloride-sensing kinase. Cellular physiology and biochemistry : international journal of experimental cellular physiology, biochemistry, and pharmacology 28, 1123–1134 (2011)10.1159/000335848).
18. Dowd BF, Forbush B, PASK (proline-alanine-rich STE20-related kinase), a regulatory kinase of the Na-K-Cl cotransporter (NKCC1). The Journal of biological chemistry 278, 27347–27353 (2003); published online EpubJul 25 (10.1074/jbc.M301899200). [PubMed: 12740379]
19. Wu QQ, Liu XY, Xiong LX, Shang JY, Mai XY, Pang RP, Su YX, Yu BX, Yuan JN, Yang C, Wang YL, Zhou P, Lv XF, Liu J, Zhou JG, Liang SJ, Reduction of Intracellular Chloride Concentration Promotes Foam Cell Formation. Circulation journal : official journal of the Japanese Circulation Society 80, 1024–1033 (2016)10.1253/circj.CJ-15-1209).
20. Darman RB, Forbush B, A regulatory locus of phosphorylation in the N terminus of the Na-K-Cl cotransporter, NKCC1. The Journal of biological chemistry 277, 37542–37550 (2002); published online EpubOct 04 (10.1074/jbc.M206293200). [PubMed: 12145304]
21. Ponce-Coria J, San-Cristobal P, Kahle KT, Vazquez N, Pacheco-Alvarez D, de Los Heros P, Juarez P, Munoz E, Michel G, Bobadilla NA, Gimenez I, Lifton RP, Hebert SC, Gamba G, Regulation of NKCC2 by a chloride-sensing mechanism involving the WNK3 and SPAK kinases. Proceedings of the National Academy of Sciences of the United States of America 105, 8458–8463 (2008); published online EpubJun 17 (10.1073/pnas.0802966105). [PubMed: 18550832]
22. Pacheco-Alvarez D, Cristobal PS, Meade P, Moreno E, Vazquez N, Munoz E, Diaz A, Juarez ME, Gimenez I, Gamba G, The Na+:Cl− cotransporter is activated and phosphorylated at the amino-terminal domain upon intracellular chloride depletion. The Journal of biological chemistry 281, 28755–28763 (2006); published online EpubSep 29 (10.1074/jbc.M603773200). [PubMed: 16887815]

23. Shcheynikov N, Son A, Hong JH, Yamazaki O, Ohana E, Kurtz I, Shin DM, Muallem S, Intracellular Cl− as a signaling ion that potently regulates Na+/HCO3− transporters. Proceedings of the National Academy of Sciences of the United States of America 112, E329–337 (2015); published online EpubJan 20 (10.1073/pnas.1415673112). [PubMed: 25561556]
24. Shekarabi M, Zhang J, Khanna AR, Ellison DH, Delpire E, Kahle KT, WNK Kinase Signaling in Ion Homeostasis and Human Disease. Cell metabolism 25, 285–299 (2017); published online EpubFeb 07 (10.1016/j.cmet.2017.01.007). [PubMed: 28178566]
25. Park HW, Nam JH, Kim JY, Namkung W, Yoon JS, Lee JS, Kim KS, Venglovecz V, Gray MA, Kim KH, Lee MG, Dynamic regulation of CFTR bicarbonate permeability by [Cl-]i and its role in pancreatic bicarbonate secretion. Gastroenterology 139, 620–631 (2010); published online EpubAug (10.1053/j.gastro.2010.04.004). [PubMed: 20398666]
26. Ohana E, Shcheynikov N, Park M, Muallem S, Solute carrier family 26 member a2 (Slc26a2) protein functions as an electroneutral SOFormula/OH−/Cl− exchanger regulated by extracellular Cl. The Journal of biological chemistry 287, 5122–5132 (2012); published online EpubFeb 10 (10.1074/jbc.M111.297192). [PubMed: 22190686]
27. Dutzler R, Campbell EB, Cadene M, Chait BT, MacKinnon R, X-ray structure of a ClC chloride channel at 3.0 A reveals the molecular basis of anion selectivity. Nature 415, 287–294 (2002); published online EpubJan 17 (10.1038/415287a). [PubMed: 11796999]
28. Bergsdorf EY, Zdebik AA, Jentsch TJ, Residues important for nitrate/proton coupling in plant and mammalian CLC transporters. The Journal of biological chemistry 284, 11184–11193 (2009); published online EpubApr 24 (10.1074/jbc.M901170200). [PubMed: 19261613]
29. Zdebik AA, Zifarelli G, Bergsdorf EY, Soliani P, Scheel O, Jentsch TJ, Pusch M, Determinants of anion-proton coupling in mammalian endosomal CLC proteins. The Journal of biological chemistry 283, 4219–4227 (2008); published online EpubFeb 15 (10.1074/jbc.M708368200). [PubMed: 18063579]
30. Lee MG, Ohana E, Park HW, Yang D, Muallem S, Molecular mechanism of pancreatic and salivary gland fluid and HCO3 secretion. Physiological reviews 92, 39–74 (2012); published online EpubJan (10.1152/physrev.00011.2011). [PubMed: 22298651]
31. Kahle KT, Delpire E, Kinase-KCC2 coupling: Cl− rheostasis, disease susceptibility, therapeutic target. Journal of neurophysiology 115, 8–18 (2016); published online EpubJan 01 (10.1152/jn.00865.2015). [PubMed: 26510764]
32. Hadchouel J, Ellison DH, Gamba G, Regulation of Renal Electrolyte Transport by WNK and SPAK-OSR1 Kinases. Annual review of physiology 78, 367–389 (2016)10.1146/annurev-physiol-021115-105431).
33. Shirakabe K, Priori G, Yamada H, Ando H, Horita S, Fujita T, Fujimoto I, Mizutani A, Seki G, Mikoshiba K, IRBIT, an inositol 1,4,5-trisphosphate receptor-binding protein, specifically binds to and activates pancreas-type Na+/HCO3− cotransporter 1 (pNBC1). Proceedings of the National Academy of Sciences of the United States of America 103, 9542–9547 (2006); published online EpubJun 20 (10.1073/pnas.0602250103). [PubMed: 16769890]
34. Yang D, Li Q, So I, Huang CL, Ando H, Mizutani A, Seki G, Mikoshiba K, Thomas PJ, Muallem S, IRBIT governs epithelial secretion in mice by antagonizing the WNK/SPAK kinase pathway. The Journal of clinical investigation 121, 956–965 (2011); published online EpubMar (10.1172/JCI43475). [PubMed: 21317537]
35. Park S, Shcheynikov N, Hong JH, Zheng C, Suh SH, Kawaai K, Ando H, Mizutani A, Abe T, Kiyonari H, Seki G, Yule D, Mikoshiba K, Muallem S, Irbit mediates synergy between ca(2+) and cAMP signaling pathways during epithelial transport in mice. Gastroenterology 145, 232–241 (2013); published online EpubJul (10.1053/j.gastro.2013.03.047). [PubMed: 23542070]
36. Hong JH, Yang D, Shcheynikov N, Ohana E, Shin DM, Muallem S, Convergence of IRBIT, phosphatidylinositol (4,5) bisphosphate, and WNK/SPAK kinases in regulation of the Na+-HCO3− cotransporters family. Proceedings of the National Academy of Sciences of the United States of America 110, 4105–4110 (2013); published online EpubMar 05 (10.1073/pnas.1221410110). [PubMed: 23431199]
37. Devogelaere B, Beullens M, Sammels E, Derua R, Waelkens E, van Lint J, Parys JB, Missiaen L, Bollen M, De Smedt H, Protein phosphatase-1 is a novel regulator of the interaction between

IRBIT and the inositol 1,4,5-trisphosphate receptor. Biochem J 407, 303–311 (2007); published online EpubOct 15 (10.1042/BJ20070361). [PubMed: 17635105]

38. Kawaai K, Mizutani A, Shoji H, Ogawa N, Ebisui E, Kuroda Y, Wakana S, Miyakawa T, Hisatsune C, Mikoshiba K, IRBIT regulates CaMKIIalpha activity and contributes to catecholamine homeostasis through tyrosine hydroxylase phosphorylation. Proceedings of the National Academy of Sciences of the United States of America 112, 5515–5520 (2015); published online EpubApr 28 (10.1073/pnas.1503310112). [PubMed: 25922519]
39. Lee SK, Boron WF, Parker MD, Relief of autoinhibition of the electrogenic Na-HCO(3) [corrected] cotransporter NBCe1-B: role of IRBIT vs.amino-terminal truncation. American journal of physiology. Cell physiology 302, C518–526 (2012); published online EpubFeb 01 (10.1152/ajpcell.00352.2011). [PubMed: 22012331]
40. Isobe K, Jung HJ, Yang CR, Claxton J, Sandoval P, Burg MB, Raghuram V, Knepper MA, Systems-level identification of PKA-dependent signaling in epithelial cells. Proceedings of the National Academy of Sciences of the United States of America 114, E8875–E8884 (2017); published online EpubOct 17 (10.1073/pnas.1709123114). [PubMed: 28973931]
41. Gross E, Fedotoff O, Pushkin A, Abuladze N, Newman D, Kurtz I, Phosphorylation-induced modulation of pNBC1 function: distinct roles for the amino- and carboxy-termini. The Journal of physiology 549, 673–682 (2003); published online EpubJun 15 (10.1113/jphysiol.2003.042226). [PubMed: 12730338]
42. Bae JS, Koo NY, Namkoong E, Davies AJ, Choi SK, Shin Y, Jin M, Hwang SM, Mikoshiba K, Park K, Chaperone stress 70 protein (STCH) binds and regulates two acid/base transporters NBCe1-B and NHE1. The Journal of biological chemistry 288, 6295–6305 (2013); published online EpubMar 01 (10.1074/jbc.M112.392001). [PubMed: 23303189]
43. Bonisch H, Runkel F, Roubert C, Giros B, Bruss M, The human desipramine-sensitive noradrenaline transporter and the importance of defined amino acids for its function. Journal of autonomic pharmacology 19, 327–333 (1999); published online EpubDec ([PubMed: 10961738]
44. Kantcheva AK, Quick M, Shi L, Winther AM, Stolzenberg S, Weinstein H, Javitch JA, Nissen P, Chloride binding site of neurotransmitter sodium symporters. Proceedings of the National Academy of Sciences of the United States of America 110, 8489–8494 (2013); published online EpubMay 21 (10.1073/pnas.1221279110). [PubMed: 23641004]
45. Jennings ML, Evidence for a second binding/transport site for chloride in erythrocyte anion transporter AE1 modified at glutamate 681. Biophysical journal 88, 2681–2691 (2005); published online EpubApr (10.1529/biophysj.104.056812). [PubMed: 15653731]
46. Santos-Sacchi J, Song L, Chloride Anions Regulate Kinetics but Not Voltage-Sensor Qmax of the Solute Carrier SLC26a5. Biophysical journal 110, 2551–2561 (2016); published online EpubJun 07 (10.1016/j.bpj.2016.05.002). [PubMed: 27276272]
47. Wu M, Heneghan JF, Vandorpe DH, Escobar LI, Wu BL, Alper SL, Extracellular Cl(−) regulates human SO4 (2-)/anion exchanger SLC26A1 by altering pH sensitivity of anion transport. Pflugers Archiv: European journal of physiology 468, 1311–1332 (2016); published online EpubAug (10.1007/s00424-016-1823-8). [PubMed: 27125215]
48. Ando H, Mizutani A, Kiefer H, Tsuzurugi D, Michikawa T, Mikoshiba K, IRBIT suppresses IP3 receptor activity by competing with IP3 for the common binding site on the IP3 receptor. Molecular cell 22, 795–806 (2006); published online EpubJun 23 (10.1016/j.molcel.2006.05.017). [PubMed: 16793548]
49. Huynh KW, Jiang J, Abuladze N, Tsirulnikov K, Kao L, Shao X, Newman D, Azimov R, Pushkin A, Zhou ZH, Kurtz I, CryoEM structure of the human SLC4A4 sodium-coupled acid-base transporter NBCe1. Nature communications 9, 900 (2018); published online EpubMar 2 (10.1038/s41467-018-03271-3).

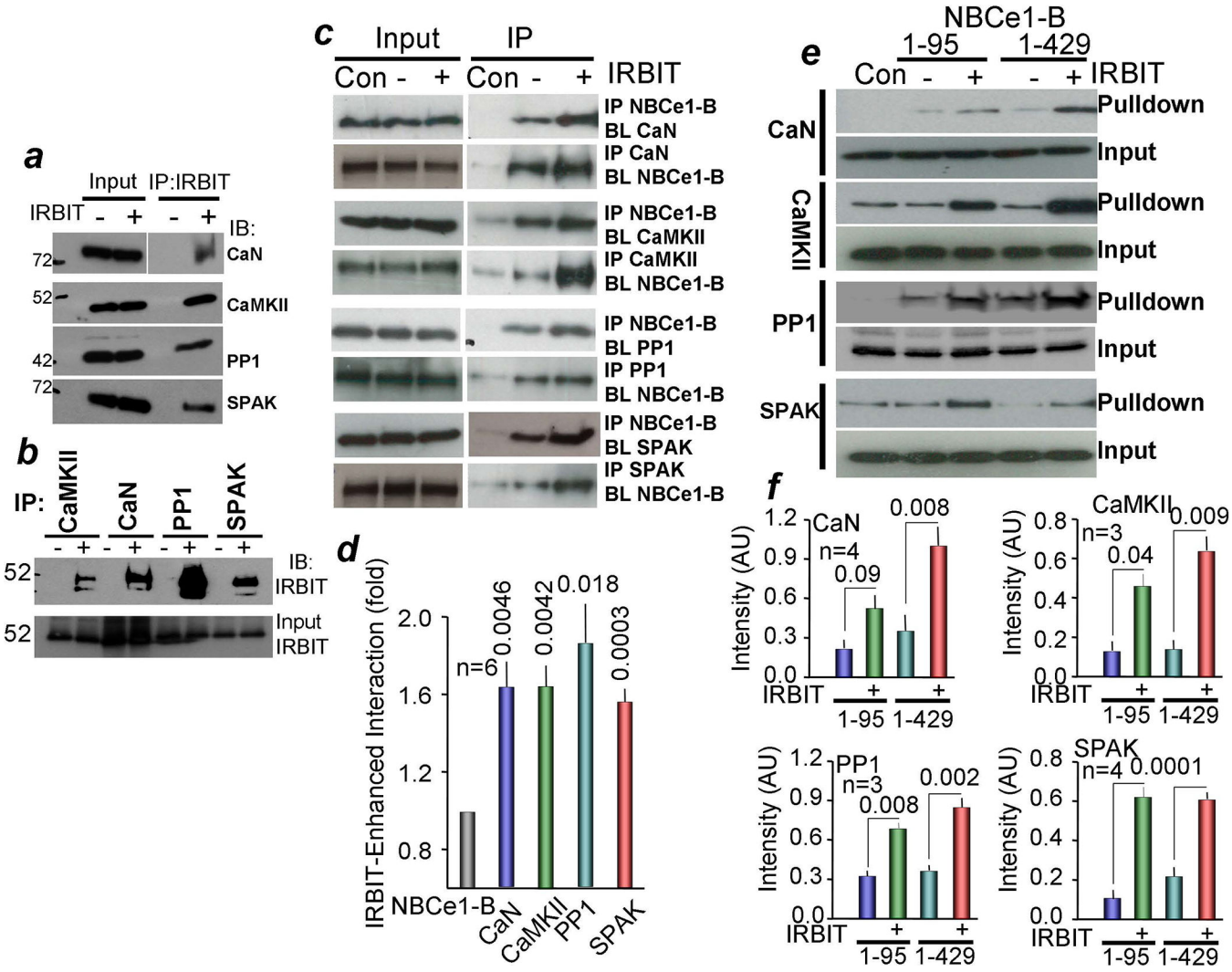

Fig. 1: IRBIT interacts with and recruits kinases and phosphatases to the NBCe1-B AID.

(**a, b**), The indicated immunoprecipitates prepared from lysates from HEK cells transfected with IRBIT and CaN, CaMKII, PP1 or SPAK were immunoblotted for the indicated proteins. (**c**), The indicated immunoprecipitates prepared from lysates from HEK cells transfected with NBCe1-B and with and without IRBIT and the indicated kinases and phosphatases were immunoblotted as indicated. In the controls (Con) precipitating antibodies were not added. (**d**) the mean±s.e.m of IRBIT-enhanced coimmunoprecipitates were determined from six similar experiments and normalized to coimmunoprecipitation in the absence of IRBIT. (**e**), lysates from HEK cells transfected with IRBIT and CaN, CaMKII, PP1 or SPAK were used for pull down with partially purified His-tagged NBCe1-B(1–95) or NBCe1-B(1–429) fragments. (**f**) the mean±s.e.m of the IRBIT-enhanced pull-down determined from 3–4 similar experiments and normalized to pull-down in the absence of IRBIT.

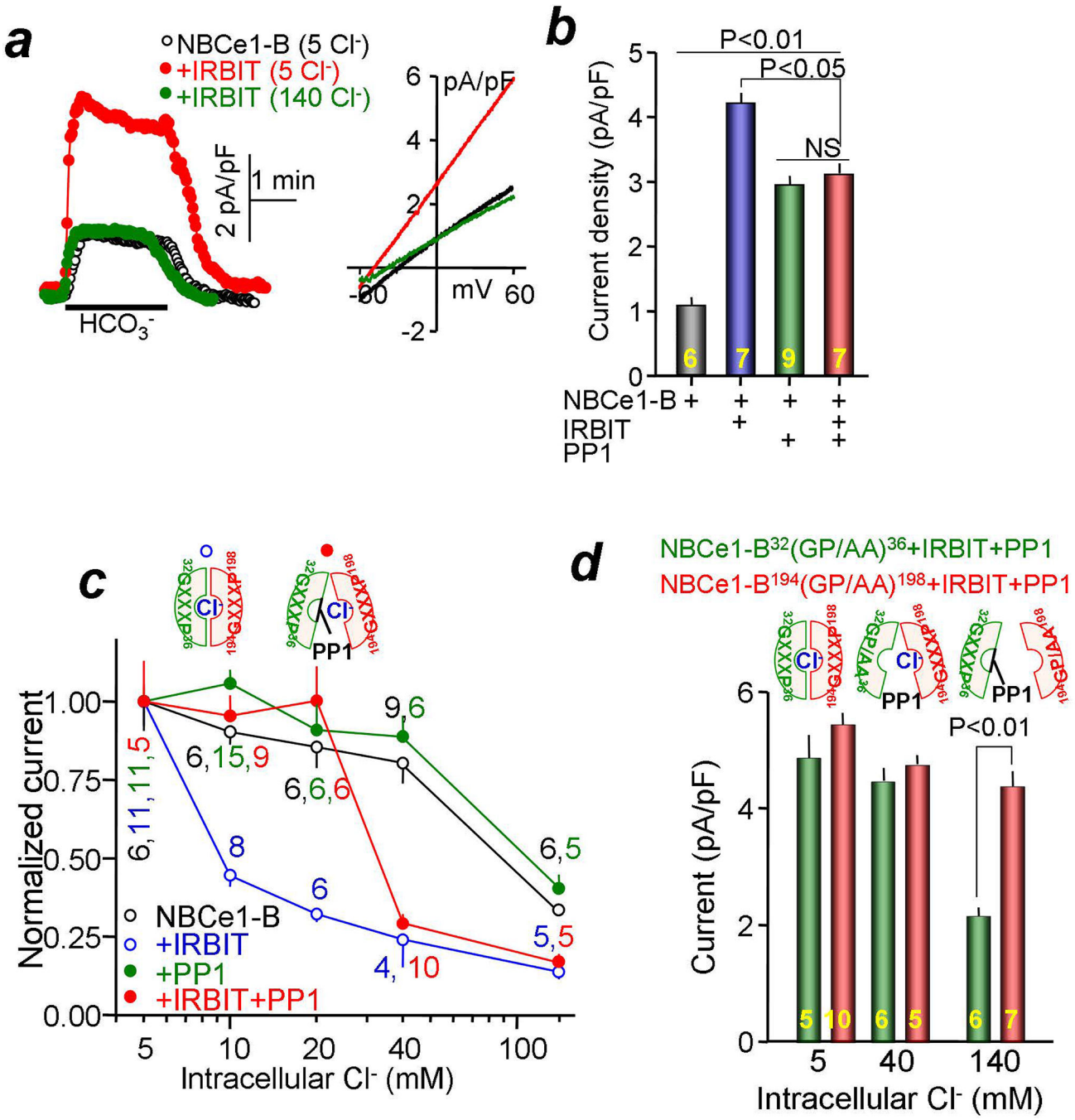

Fig. 2: PP1 acts on NBCe1-B(S^{65}) to control Cl^-_{in} sensing by the ^{32}GXXXP^{36} site.

(**a**) Example traces of current time course in response to adding bath HCO_3^- and the I/V at peak current. (**b**): HEK cells transfected with NBCe1-B and with or without IRBIT and PP1 were used to measure NBCe1-B-mediated current due to Na+−2HCO_3^- cotransport at 5 mM Cl^-_{in}. The columns show the mean±s.e.m. (**c**): Current was measured in HEK cells transfected with NBCe1-B alone (black), with PP1 (green), IRBIT (blue), or IRBIT and PP1 (red) and pipette solutions containing the indicated Cl^- concentrations. Normalized current is shown to illustrate the effect of IRBIT. (**d**): Current was measured in HEK cells

transfected with the mutants NBCe1-B(^{32}GP/AA^{36}) (green) or NBCe1-B(^{194}GP/AA^{198}) together with IRBIT and PP1 at pipette solutions containing 5, 40 or 140 mM Cl^-. The models in (c, d) depict the effect of the indicated condition on the state of Cl^- sensing. Close GXXXP motifs indicates Cl^- sensing by both motifs and inhibition by Cl^-_{in} at high affinity, partially open GXXXP motifs indicates loss of Cl^- sensing by one GXXXP motif and Cl^- sensing by the available motif al low affinity, and fully open GXXXP motifs indicating complete loss of Cl^-_{in} sensing. The numbers in the columns and next to the symbols indicate the number of current measurements and the results are given as mean±s.e.m.

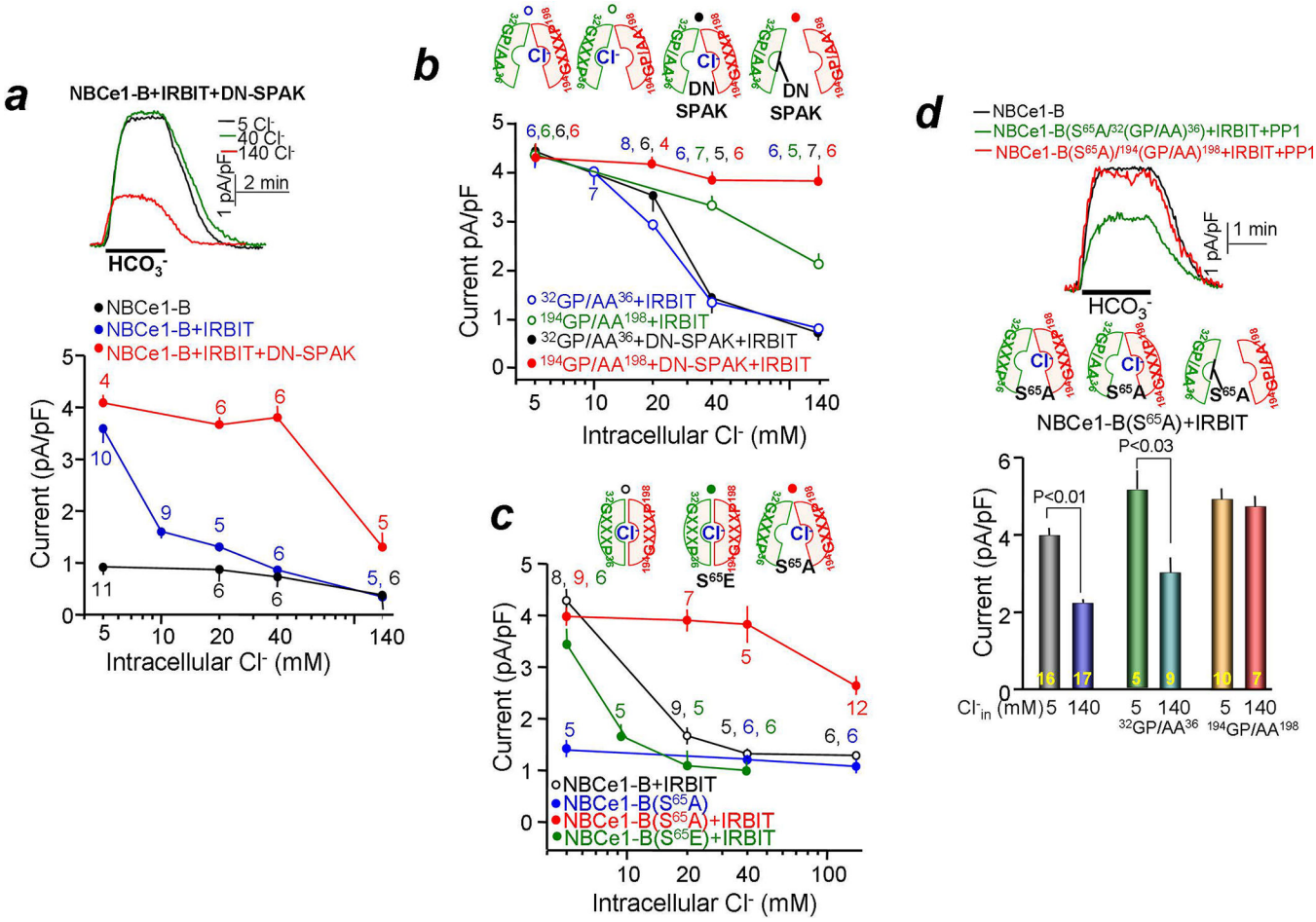

Fig. 3: SPAK acts on NBCe1-B(S^{65}) to control Cl'm sensing by the ^{32}GXXXP^{36} site.

(**e-d**): Current was measured in HEK cells transfected with wild-type NBCe1-B and IRBIT (**a, c**), NBCe1-B(^{32}GP/AA^{36}) or NBCe1-B(^{194}GP/AA^{198}) and IRBIT (**b, d**), or NBCe1-B(S^{65}E) and IRBIT (c) NBCe1-B(S^{65}A) alone or with IRBIT (c, d), and NBCe1-B, IRBIT and dominant negative (DN) SPAK (a, b) and with pipette solutions containing the indicated Cl^- concentrations. Example of current traces at the indicated Cl^-_{in} concentrations and the indicated NBCe1-B mutants are shown in (**a, d**). The models in (**b-d**) depict the effect of the indicated conditions on the state of Cl^- sensing by the GXXXP motifs. The numbers in the columns and next to the symbols indicate the number of current measurements and the results are given as mean±s.e.m.

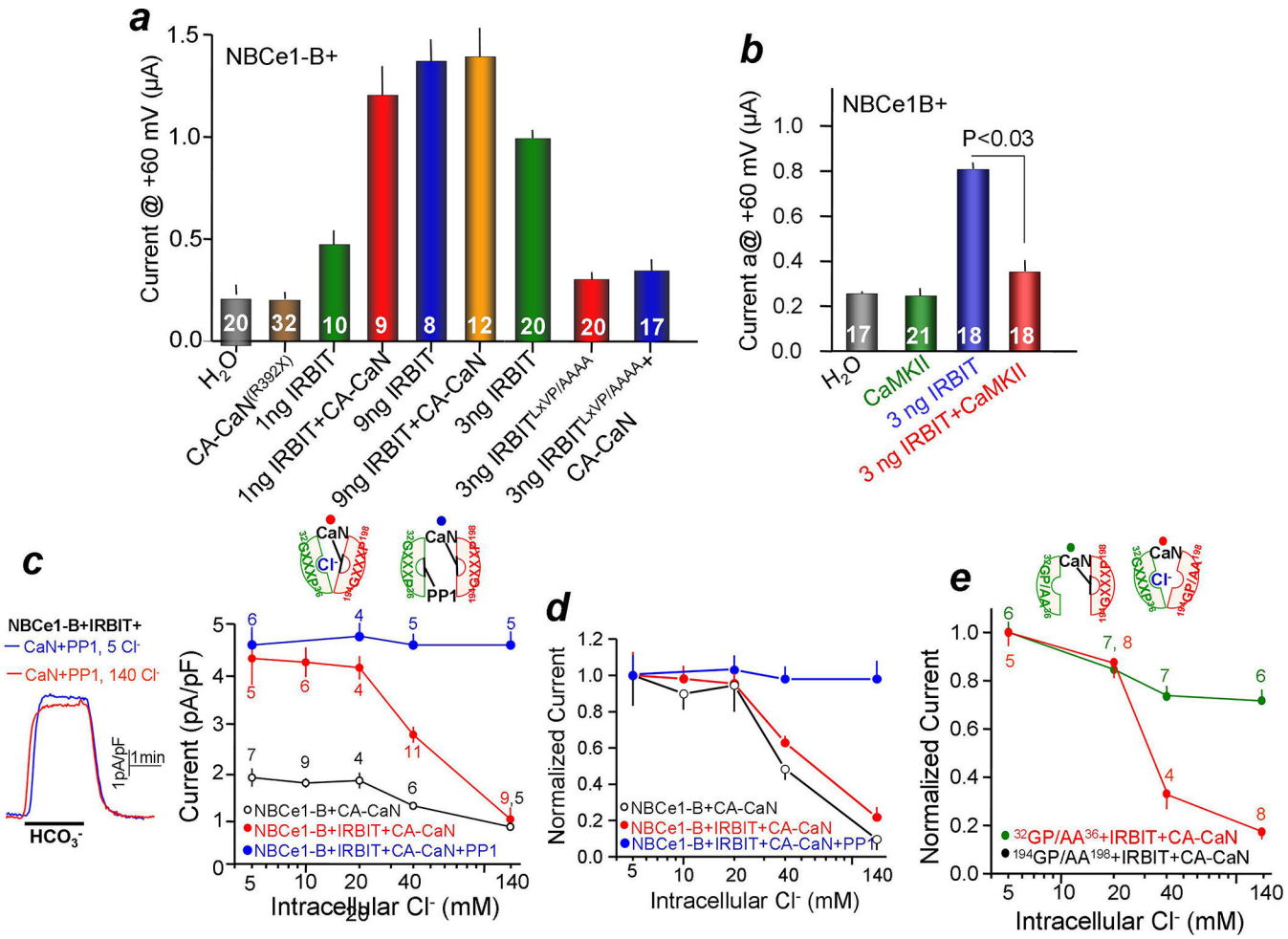

Fig. 4: CaN and CaMKII regulates NBCe1-B activity and CaN controls Cl^-_{in} sensing by the ^{194}GXXXP^{198} motif.

(**a**): Current was measured in *Xenopus* oocytes injected with cRNAs coding for NBCe1-B and H2O (black), constitutively active (CA) CaN^{R392X} (brown), the indicated ng of IRBIT, the IRBIT($^{LxVP/AAAA}$) mutant alone or together with CA-CaN. (**b**): Same as in (a), except that the oocytes were injected with cRNA coding for CaMKII, IRBIT or IRBIT+CaMKII. (**c-e**): Current was measured in HEK cells transfected with NBCe1-B (**c, d**), NBCe1-B(^{32}GP/AA^{36}) or NBCe1-B(^{194}GP/AA^{198}) (**e**) and CA-CaN (**c-e**) or CA-CaN+PP1 (blue in **c, d**). (**d**) shows normalized current in (d). The models in (c, e) depict the effect of the indicated condition on the state of Cl^- sensing by the GXXXP motifs. The numbers in the columns and next to the symbols indicate the number of current measurements and the results are given as mean±s.e.m.

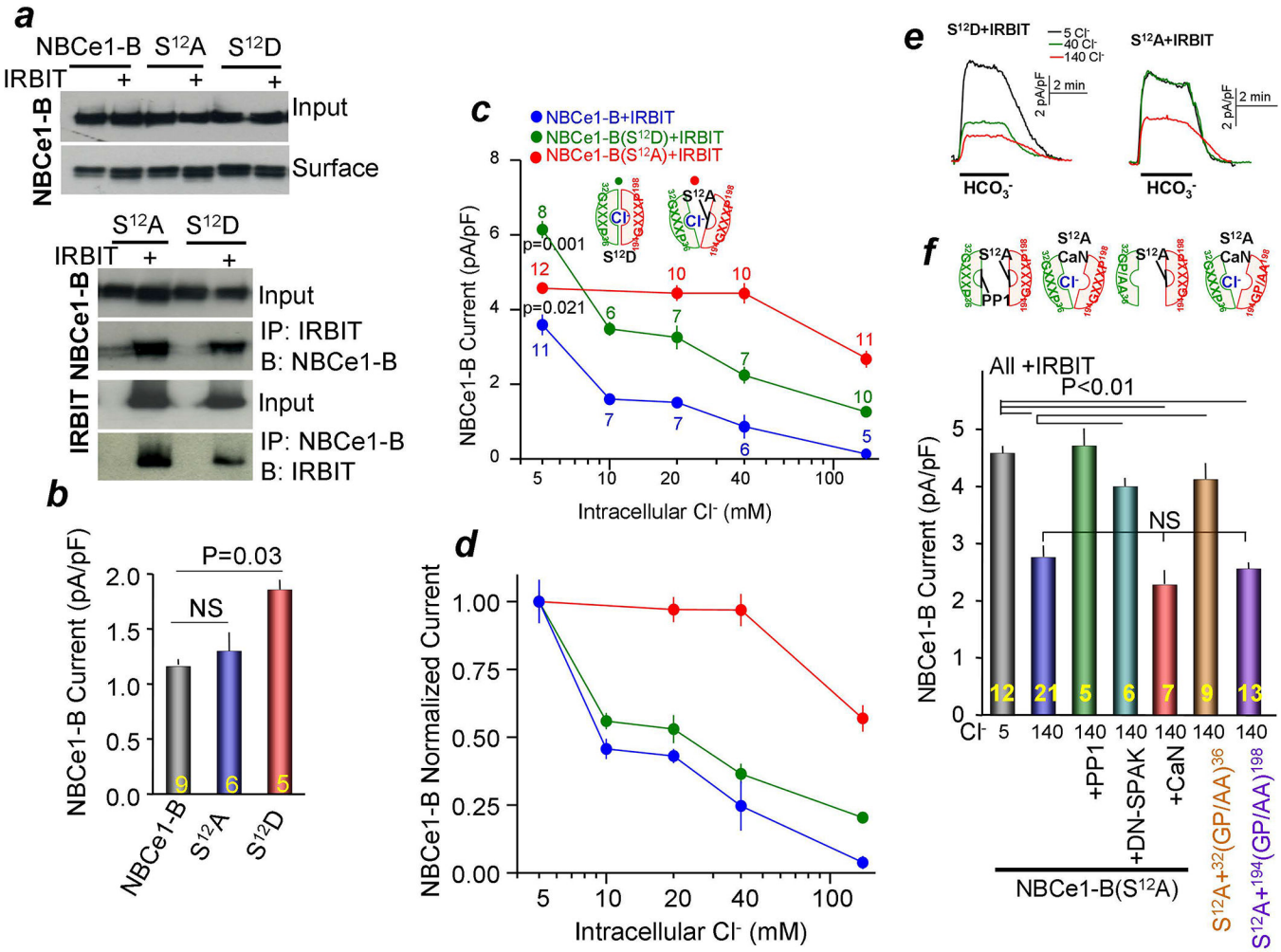

Fig. 5: CaN acts on NBCe1-B(S12) to control Cl^-_{in} sensing by the ^{194}GXXXP^{198} motif.

Panel (**a**): Effect of the S^{12}A and S^{12}D mutations on NBCe1-B surface expression and interaction with IRBIT (n=3). (**b-d**): Effect of S^{12}D and S^{12}A mutations on the activity of NBCe1-B measured at 5 mM Cl^-_{in} (**b**), and increasing concentrations of Cl^-_{in} (**c, d**). The current in (**c**) is shown as normalized current in (**d**). (**e**): Example current traces measured in cells expressing NBCe1-B(S^{12}D) or NBCe1-B(S^{12}A) and the indicated Cl^-_{in}. (**f**): NBCe1-B(S^{12}A) current was measured in the presence of 5 or 140 mM pipette solution in HEK cells expressing NBCe1-B(S^{12}A) alone (gray and blue) or together with PP1 (green), DN-SPAK (turquoise) or CaN (red). Current was measured with the double mutants NBCe1-B(S^{12}A/^{32}GP/AA^{36}), brown) or NBCe1-B(S^{12}A/^{194}GP/AA^{198}), purple). The models in (**c, f**) depict the effect of the indicated condition on the state of Cl^- sensing by the GXXXP motifs. The numbers in the columns and next to the symbols indicate the number of current measurements and the results are given as mean±s.e.m.

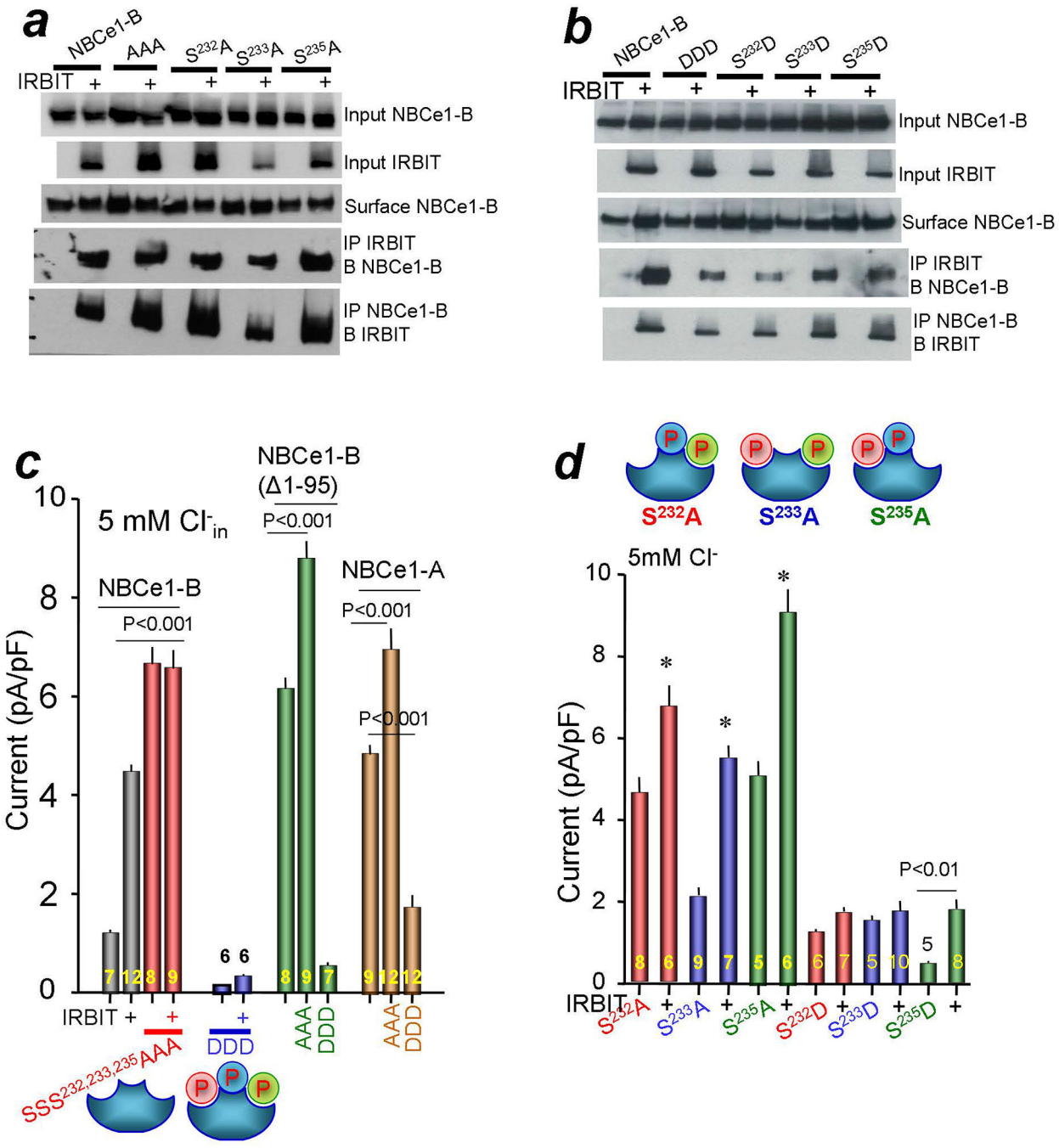

Fig. 6: IRBIT-dependent dephosphorylation of S^{232}, S^{233} and/or S^{235} affect NBCe1-B activity and activation by IRBIT.

(**a, b**): The effect of the S^{232}, S^{233} and/or S^{235} mutations on NBCe1-B surface expression and interaction with IRBIT (n=4). (**c, d**): Current was measured with pipette solution containing 5 mM Cl^- and in the presence (+) or absence of IRBIT, as indicated. The cells were transfected with (**c**) NBCe1-B (gray), NBCe1-B(SSS/AAA) (red), NBCe1-B(SSS/DDD) (blue), NBCe1-A and its AAA and DDD mutants, NBCe1-B(Δ1–95) and its AAA and DDD mutants, (**d**) S^{232}A or S^{232}D (red), S^{233}A or S^{233}D (blue) and S^{235}A or S^{235}D

(green). The models in (**c, d**) depict the phosphorylation state of S^{232}, S^{233} and S^{235} for the indicated mutants. * denotes $p<0.01$ relative to no IRBIT. The numbers in the columns indicate the number of current measurements and the results are given as mean±s.e.m.

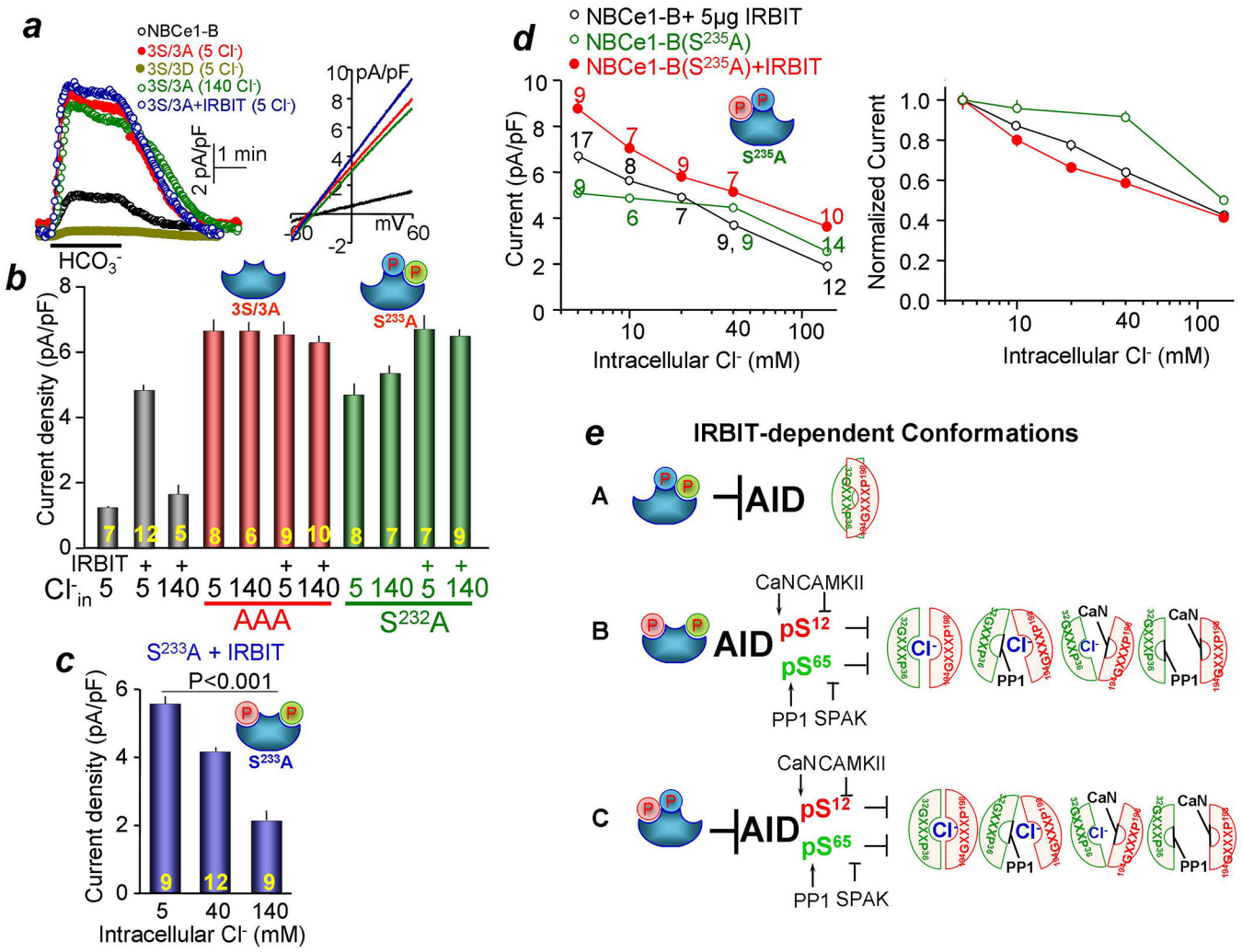

Fig. 7: S^{232} affects NBCe1-B Cl^-_{in} sensing.

(**a**) Example traces of current time course in response to adding bath HCO_3^- measured in HEK cells transfected with NBCe1-B, NBCe1-B+IRBIT or the mutant $S^{232}A/S^{233}A/S^{235}A$ (3S/3A), 3S/3A+IRBIT and 3S/3D with pipette solution containing 5 or 140 mM Cl^- and the I/V at peak current. (**b**): Shows the current of NBCe1-B (gray), the SSS/AAA (red) and the $S^{232}A$ (green) mutants in the presence (+) or absence of IRBIT measured at 5 and 140 mM Cl^-_{in}. (**c**) shows the current of NBCe1-B(S233A)+IRBIT at 5, 40 and 140 mM Cl^-_{in}. (**d**) The effect of Cl^-_{in} on current measured with NBCe1-B+ saturating 5 µg IRBIT (black), NBCe1-B($S^{235}A$) alone (green) or with 1 µg IRBIT (red). The right plot shows the normalized current in the left plot. (**e**) A model of the three IRBIT-dependent NBCe1-B conformations and their properties with respect to autoinhibition, Cl^-_{in} sensing and regulation of Cl^-_{in} sensing by the PP1/SPAK and CaN/CaMKII. The models in (**b-e**) depict the phosphorylation state of S^{232}, S^{233} and S^{235} and Cl^-_{in} sensing by the GXXXP motifs of each mutant. The numbers in the columns indicate the number of current measurements and the results are given as mean±s.e.m.